HHS Public Access

Author manuscript

Reprod Toxicol. Author manuscript; available in PMC 2018 July 06.

Published in final edited form as:

Reprod Toxicol. 2018 June ; 78: 20–28. doi:10.1016/j.reprotox.2018.03.001.

Estrous cycle-dependent modulation of *in vivo* microvascular dysfunction after nanomaterial inhalation

P.A. Stapleton[a,b,*], **C.R. McBride**[c,d], **J. Yi**[c], **A.B. Abukabda**[c,d], and **T.R. Nurkiewicz**[c,d]

[a]Department of Pharmacology and Toxicology, Ernest Mario School of Pharmacy, Rutgers University, Piscataway, NJ, USA

[b]Environmental and Occupational Health Sciences Institute, Piscataway, NJ, USA

[c]Department of Physiology, Pharmacology, and Neuroscience, West Virginia University, Morgantown, WV, USA

[d]Toxicology Working Group, West Virginia University, Morgantown, WV, USA

Abstract

Preconceptive health encompasses male and female reproductive capability. In females, this takes into account each of the stages of the estrous cycle. Microvascular reactivity varies throughout the estrous cycle in response to hormonal changes and in preparation for pregnancy. Microvascular alterations in response to engineered nanomaterial (ENM) exposure have been described within 24-h of inhalation; however, the impact upon the uterine vasculature at differing estrous stages and at late-stage pregnancy is unclear. Female Sprague Dawley (SD) rats (virgin and late stage pregnancy [GD 19]) were exposed to nano-TiO aerosols (173.2 ± 6.4 nm, 10.2 ± 0.46 mg/m^3, 5 h) 24-h prior to experimentation leading to a single calculated deposition of 42.2 ± 1.9 μg nano- TiO_2 (exposed) or 0μg (control). Animals were anesthetized, estrous status verified, and prepared for *in situ* assessment of leukocyte trafficking and vascular function by means of intravital microscopy, Uterine basal arteriolar reactivity was stimulated using iontophoretically applied chemicals: acetylcholine (ACh, 0.025 M; 20, 40, 100, 200 nA), sodium nitroprusside (SNP, 0.05 M; 20, 40, 100 nA), phenylephrine (PE, 0.05 M; 20, 40, 100 nA). Finally, adenosine (ADO, 10^{-4} M) was superfused over the tissue to identify maximum diameter. *In situ* vessel reactivity after exposure was significantly blunted based on estrous stage, but not at late-stage pregnancy. Local uterine venular leukocyte trafficking and systemic inflammatory markers were also significantly affected during preparatory (proestrus), fertile (estrus), and infertile (diestrus) periods after ENM inhalation. Overall, these deficits in reactivity and increased inflammatory activity may impair female fertility after ENM exposure.

*Corresponding author at: Department of Pharmacology and Toxicology, Ernest Mario School of Pharmacy, Environmental and Occupational Health Sciences Institute, Rutgers University, 170 Frelinghuysen Road, Piscataway, NJ, 08854, USA. stapleton@eohsi.rutgers.edu (P.A. Stapleton).

Conflict of interest

The authors report no conflict of interest.

Keywords

Engineered nanomaterials; Nanotoxicology; *in vivo*; Intravital microscopy; Estrous cycle; Uterus; Basal uterine arterioles

1. Introduction

Given the epidemiological associations of elevated air pollution with increased rates of respiratory and cardiovascular morbidity and mortality [1,2], many studies have focused on the cardiovascular implications of burning biomass, urban/industrial sources of air pollution, and the burgeoning use of engineered nanomaterials (ENM). However, air pollution exposure and associated cardiovascular impairments may lead to effects in other physiological systems, including the reproductive and immune systems.

Recently, investigators have sought to identify the impact of air pollution exposure on preconceptive health and fertility. Reviews and data meta-analyses have concluded that air pollution exposure can have a significant impact on fertility and miscarriage rates in normal and subfertile populations [3,4]. The Nurses' Study II, a prospective cohort study, recently identified air pollution exposure as a risk for infertility [5]. Additional studies associate exposure to high levels of particulate matter (PM) with early pregnancy loss among couples naturally conceiving or undergoing fertility treatment [6,7]. These outcomes have been associated with defects in gametogenesis [8]. Ongoing investigations suggest associations between air pollution and deficits in sperm quality, motility, morphology, and count [9–12], while the physiological effects on the female reproductive system have been essentially unexplored [13].

Given the complex mixture of chemicals, gases, and materials in air pollution [14] and the increased toxicities associated within the ultrafine fraction (<0.1 μm) of air pollution [15], ENM have been introduced as a surrogate for ultrafine PM to enable toxicological analysis to a homogeneous nanoscale particulate [16]. Despite the rapidly increasing commercial use of nanomaterials, few groups have sought to identify the potential reproductive and developmental toxicities associated with ENM exposures during gestation [13,17–19] and even less is known about outcomes of exposure prior to conception.

Understanding of uterine microcirculation reactivity during estrous and pregnancy is limited [20]. Anatomically, female human and rodent reproductive anatomy differs vastly, as rodents possess a dual-horn uterus to allow for multiple pup litters. However, there are hormonal similarities marked by elevated estrogen and a spike of luteinizing hormone leading to ovulation in both species [21,22]. The ability of the supporting vasculature to meet the demands of the maternofetal unit is critical for a successful pregnancy. Our previous work has identified uterine microvascular dysfunction in the pregnant [23] and virgin (diestrus) rat [24] after inhalation of ENM. These studies indicate the ability of pulmonary xenobiotic exposure to impair uterine microvascular function, leading to dysfunction of normal uterine physiological functions [e.g. preparation of the uterine lining for implantation (growth, clearance of waste) or support of ongoing pregnancy]. However, these observations address only a brief snapshot of the female reproductive cycle. Hormone fluctuations during the

estrous cycle may influence microvascular reactivity, inflammatory action, and subsequent fertility [25]; consequently, each stage must be evaluated independently.

Xenobiotic pulmonary exposures are theorized to ignite both systemic and local inflammation [14]. Systemic inflammation may develop through initial pulmonary insult leading to the production of circulating cyto- and chemokines; while local inflammation may develop due to particle translocation and deposition from the site of original exposure.

The purpose of the present studies was to identify acute *in situ* uterine microvascular reactivity responses throughout the estrous cycle following a single ENM pulmonary exposure. Using intravital microscopy techniques, we can evaluate these stages independently while maintaining normal humoral perfusion and neural innervation [24]. Lastly, we conducted measures of systemic inflammation and local uterine leukocyte trafficking.

2. Materials and methods

2.1. Animal model

Female Sprague-Dawley (SD) rats were purchased from Hilltop Laboratories (Scottsdale, PA), and provided food and water *ad libitum*. They were acclimated for 72 h prior to use and were randomly assigned to either the naive, control, or exposure groups. Estrous status was verified by microscopic evaluation of vaginal smears immediately prior to surgery [23–26]. Rats within the late-stage pregnancy cohort mated in-house. Successful mating was assured based on the presence of sperm in the vaginal canal and the date was identified as GD 1. These animals were monitored for increased weight during their pregnancy and remained in the animal facility until GD 19 for exposure and GD 20 for surgery, as previously described [23,27,28]. All procedures were approved by the Institutional Animal Care and Use Committee of West Virginia University.

2.2. Particle characterization

Nanosized TiO_2 P25 was obtained from Evonik (Aeroxide TiO_2, Parsippany, NJ) and prepared prior to aerosolization by drying, sieving and storing the powder [29,30]. It has previously been shown to be a mixture composed primarily of anatase (80%) and rutile (20%) TiO_2, with a primary particle size of 21 nm and a mean surface area of 48.08 m^2/g [30–32].

2.3. Inhalation exposure

Our nanoparticle aerosol generator was designed and tested specifically for rodent nanoparticle inhalation exposures (US Patent No. 8881997) [33,34]. As previously described, nano-TiO_2 aerosols generated from the bulk dry powder were diluted and delivered to the inhalation exposure chamber [23,24]. The aerosol characteristics were monitored in real time and manually adjusted to assure a consistent and known exposure for each experimental animal using an Electrical Low Pressure Impactor (ELPI; Dekati, Tempere, Finland) and Scanning Mobility Particle Sizer (SMPS; TSI Inc, St. Paul, MN).

Non-pregnant and gestational day (GD) 19 pregnant rats were placed singly in the whole-body exposure chamber with a volume of 500 L [34] for 5-h during the single nano-TiO_2 inhalation exposure. Exposures were initiated between 9am and 11am, approximately 24-h prior to microvascular assessments to maintain consistency and avoid any variability associated with the rats' circadian rhythm [23,24]. Once a steady-state aerosol concentration was achieved (final mass concentration of 10.2 ± 0.46 mg/m^3 for nano-TiO_2), exposure duration was adjusted to achieve a single calculated deposition of 42.2 ± 1.9 μg nano-TiO_2 (exposed) or 0 μg (control) and final deposition of 13.3 ± 0.8 μg after normal clearance [24]. During the inhalation exposure, particles were collected onto 47 mm Teflon sheets and particle concentration was verified using gravimetric sampling [33]. Aerodynamic diameter (173.2 ± 6.4 nm; Electrical Low Pressure Impactor (ELPI), Dekati, Tempere, Finland) and particle size distribution (165.8 ± 5.4 nm; Scanning Mobility Particle Sizer (SMPS; TSI Inc., St. Paul, MN) were measured in real-time (Fig. 1). Included for study were virgin and pregnant filtered-air sham control rats and naive (not placed within the inhalation chamber) control rats.

Total deposition was calculated based on mouse methodology previously reported [35] and normalized based on rat weight and to rat minute ventilation [23,24] using the following equation: D = F*V*C*T, where F is the deposition fraction (10%), V is the minute ventilation based on body weight, C equals the steady state mass concentration (mg/m^3), and T equals the exposure duration (minutes) [30].

2.4. Surgical preparation

Surgeries were initiated between 9am and 11am, 22–26 h after the initiation of nano-TiO_2 exposures to be consistent with previous study evaluations at a 24-h time point (REFS) and to reduce circadian rhythm variability. Rats were anesthetized, estrous phase was verified, and prepared for intravital microscopy. GD 20 pregnant rats were prepared in a similar fashion (Fig. 2). The animals were anesthetized with Inactin (100 mg/mL i.p.) and placed supine on a heating pad to maintain a 37° C rectal temperature. The trachea and carotid artery were cannulated to ensure a patent airway and to monitor mean arterial pressure and heart rate. A longitudinal incision was made on the right iliac region of the abdomen and the right horn of the gravid uterus was surgically exteriorized over an optical pedestal specially designed to support the pups and for uterine transillumination. To reduce myometrial motility during the experiment, the right horn of uterus was continuously superfused (3–4mL/min) with a warmed (35° C) and equilibrated (95% N/5% CO_2) physiological salt solution (PSS; 119 mM NaCl, 25 mM $NaHCO_3$, 6 mM KCl, and 3.6 mM $CaCl_2$) with the addition of isoproterenol (10 mg/L; Sigma-Aldrich, St. Louis, MO) and phenytoin (20 mg/L; Sigma-Aldrich, St. Louis, MO) [24,36–40].

2.5. Intravital microscopy and microiontophoresis

The animal preparation was transferred to the stage of an Olympus intravital microscope (Model BX51WI, Center Valley, PA) linked to a charge-coupled device (CCD) Olympus video camera (Model DP71). Microvessels were visualized using a 20× water-immersion objective. Video images were viewed on a high-resolution color monitor and digitally

recorded via DP Controller (Olympus, Center Valley, PA) for off-line analysis (Image J) [24,41].

2.5.1. Leukocyte trafficking—After a 20-min equilibration period, leukocyte adhesion and rolling in separate second- or third-order venules were counted for 1 min in each vessel studied (2 or 3 per rat) using a 20× water immersion objective to characterize leukocyte trafficking after nano-TiO_2 exposure.

2.5.2. Vascular assessment—Micropipettes were backfilled with acetylcholine (0.025 M; ACh), sodium nitroprusside (0.05 M; SNP), or phenylephrine (0.05 M; PE). A micromanipulator (Narishige, Tokyo, Japan) was used to position the tip parallel to the arteriolar wall in order to evaluate endothelium-dependent dilation (EDD; ACh; 20, 40, 100, and 200 nA), –independent dilation (EID; SNP; 20, 40, and 100 nA), and vascular smooth muscle responsiveness (VSM; PE; 20, 40, and 100 nA). Micropipettes were connected to a current programmer (model 260; World Precision Instruments, New Haven, CT) via an Ag/AgCl wire as previously described [24]. All experimental periods were at least 2 min, steady-state diameters were collected for at least one minute, and vessels recovered back to baseline for 2–5 min after agonist administration. The chemical applications were randomized between animals to prevent any ordering effects. Passive maximum arteriolar diameter was established by superfusing the tissue with 10^{-4} M adenosine.

The responses to ACh, SNP, and PE are presented as raw measurements (micrometers, μm) and as calculated baseline active-vascular tone via the equation $T = [D_M\text{-}D_{BASE}/D_M]*1\ 00$, where D_M is the maximum diameter measured during adenosine superfusion and D_{BASE} is vessel diameter at baseline [36]. To compare across groups, we normalized chemical-dependent baseline reactivity to its maximum response, allowing for an appropriate comparison of microvascular reactivity across groups. This normalization used the following equation: $[(D_{SS}\text{-}D_{CON})/(D_M\text{-}D_{CON})]*1\ 00$, where D_{SS} is the steady-state diameter achieved after each chemical bolus, D_{CON} is the baseline diameter measured immediately prior to the microiontophoresis administration, and D_M is the maximal response after adenosine administration at the end of each experiment [23,24,36,42].

2.6. Inflammatory panels

Upon conclusion of the intravital microscopy, whole blood was collected directly from the carotid artery into EDTA vacutainers and centrifuged (1100× *g*) to separate the components. The plasma was collected, flash-frozen in liquid nitrogen, and stored at −80 °C until analysis. Rats were killed and tissues harvested for further analysis. Multi-spot inflammatory and proinflammatory assays were completed per manufacturer's directions (Meso Scale Diagnostics, Rockville, MD) for: lipocalin-2, TSP-1, TIMP-1, MCP-1, interferon (IFN)-γ, interleukin (IL)-1β, IL-4, IL-5, IL-6, KC/GRO, IL-10, IL-13, and TNF-α.

2.7. Statistical analysis

The data are expressed as mean ± standard error (SE), where "N" represents the number of rats studied and "n" represents the number of arterioles evaluated as previously described [23,30,43]. Global effects within the window of normalized vascular reactivity for each

estrous phase were independently evaluated using multiple regression analyses followed by ANOVA to denote significant differences between responses. Inflammatory panels were assessed by a two-way analysis of variance (ANOVA) and followed by Holm-Sidak post-hoc test, $p < 0.05$ was taken to reflect statistical significance.

3. Results

3.1. Vascular reactivity

To distinguish any stresses to the vascular system associated with transportation to/from the inhalation facility or noise related to the operation of the facility, two groups of controls were assessed. This included a naive group which did not enter the inhalation facility and a filtered air sham group, which were handled in the same manner as the exposed group. There were no significant differences noted between these naive (N = 15, n = 27) and sham (N = 4; n = 11) groups in response to the endothelium-dependent dilator acetylcholine (ACh) (Fig. 3); therefore, the controls presented represent a pooling of the naive and sham samples. Data indicate that the animals do not have a measureable vascular stress reaction to placement within the inhalation facility 24-h post-inhalation. With the understanding that each stage of estrous is associated with differing vascular reactivity due to hormonal fluctuations, the vascular assessments will be presented comparing the control and exposed groups within each stage of estrous and at late-stage (GD 20) pregnancy.

There were no significant differences with respect to age or body weight between the control and exposed groups in any of the estrous groups or at GD 20 of pregnancy (Table 1). Additionally, there were no significant differences between the size of the vessels between the control and exposed groups either at baseline or at maximum dilation induced by adenosine superfusion (Table 1).

Differences in endothelium-dependent reactivity were identified between estrous groups in response to increased concentrations of ACh, where reactivity during proestrus, estrus, and late stage pregnancy are significantly different than reactivity during diestrus (Table 2). These measurements demonstrate modulations of vascular response throughout the estrous cycle (Fig. 4). When response was examined over the physiological range, the rates of endothelium-dependent dilation associated with ENM exposure were significantly different during metestrus, diestrus, estrus, and late-stage pregnancy (Fig. 4). The reactivity curve during estrus, the reproductively receptive stage of the estrous cycle, constricts to increased concentrations of ACh, an endothelium-dependent dilator. If this phenomenon were to persist after conception, blood flow necessary to support normal fetal maturation might not be present, described as the development of a hostile gestational environment and supported by our previous work [20].

There were trends and significant differences in the raw vessel diameter to increased concentrations of the endothelium-independent dilator SNP associated with estrous status at the 20 nA and 40 nA concentrations, where estrus cycle stage led to significant differences in endothelium-independent reactivity between infertile periods of the estrous cycle (metestrus and diestrus as compared to late-stage pregnancy (Fig. 5). The single-stage responses between control and exposed animals were assessed to compare the reactivity

throughout the pharmacological treatment range (Fig. 5). In this case, significantly different rates of reactivity were identified in di- and proestus stages indicating a reduced ability to utilize bioavailable NO compared to control after ENM exposure. Interestingly, endothelium-dependent and - independent dilation is significantly different during pregnancy than alfor all late-pregnancy group.

There were indications of an altered sensitivity or response to α-adrenergic stimulation in the vascular smooth muscle associated with estrous status between diestrus, compared with met-or proestrus at an ionic concentration associated with 40 nA (Table 2). At this dose, vascular reactivity was also significantly different with respect to ENM exposure. When evaluated over the range of PE responses, there were no significant differences identified at any estrous stage (Fig. 6). Taken together, these findings suggest an inability to appropriately sense and react to local blood flow mediators initiating vasorelaxation.

3.2. Inflammatory mediators

A count of venular leukocyte-endothelium interactions revealed significant differences in the groups according to stage of the estrous cycle: diestrus, proestrus, and estrus, with the average observed interactions within the exposed groups significantly higher than controls (Fig. 7). This is suggestive of a proinflammatory environment within the uterus during both receptive and quiescent periods of the estrous cycle 24-h after nano-TiO_2 inhalation, a tatus which may affect conception.

Inflammatory mediators did not vary with respect to estrous phase. However, significant differences ($p = 0.016$) were identified in IL-4 concentrations between control and exposed groups (Table 3). There was also a trend toward significance between the control and exposed groups with respect to IL-6 ($p = 0.069$) and IL-13 ($p = 0.079$) (Table 3). There were no differences identified with respect to the remaining inflammatory markers evaluated 24-h after ENM inhalation. Overall, alterations to the inflammatory environment during reproductively relevant phases of estrous and pregnancy may have implications for conception and the developing fetus (Table 3–4).

4. Discussion

The present experiments identified *in situ* alterations to pre-conceptive uterine vascular reactivity 24-h after ENM inhalation at each stage of estrous, but not at late stage pregnancy. This is the first study to evaluate toxicological exposures using intravital microscopy to evaluate arteriolar function in the late-stage pregnant uterus while preserving reserving all neurological, humoral, and fetal biofeedback. ENM exposure led to a significant impairment of endothelium-dependent reactivity during estrus and late-stage pregnancy; while an increased rate of response was evident in infertile periods of estrous. Leukocyte counts between the control and exposed venules were significantly higher during preparatory (proestrus), fertile (estrus), and infertile (diestrus) periods after ENM inhalation. Additionally, levels of IL-4 were elevated in response to a single ENM inhalation exposure. Therefore, the uterine environment post-exposure may not provide a receptive environment for implantation or the initiation of a successful gestation.

The biological variability of the intact GD 20 uterus makes it difficult to conclusively identify significant differences at this stage of pregnancy, however endothelium-dependent dilation was significantly blunted in the late-stage pregnant group, indicating an inability to properly react to dilation mediators. Reduced blood flow to the fetus during late-stage pregnancy may impair nutrient-waste exchange and overall fetal growth.

While the results within the pregnancy group included some differences of reactivity within the PE and SNP ionic doses did not achieve statistical significance and varies from our previous work [23]. This may be due to study design as this study included a single inhalation exposure to nano-TiO2, versus the chronic exposures throughout gestation used previously and kept all neurological, humoral, and fetal networks intact, while previous studies to care to evaluate isolated microvessels of the uterine circulation. Interestingly, in a different cohort of animals focusing intravital *in situ* methodology solely during the diestrus stage of the estrus cycle [24], the patterns of reactivity within those groups of animals were nearly identical to the findings presented here, affirming reproducibility, validity, and reliability to these exposures and methodologies.

The roles of inflammatory mediators in preconceptive, conceptive, and gestational health are not well defined; however, it is becoming clear that inflammatory elevations and reductions are crucial for proper endometrial function and successful implantation. Elevated concentrations of IL-6 in humans have been associated with preterm birth [44]. Interestingly, the level of IL-6 in this study was significantly elevated at late pregnancy after ENM exposure. Given the roles immunity and inflammation play in successful implantation, placental development, and gestation [45], dysfunction of preconceptive and perinatal regulation of these mediators may lead to infertility [46,47] and altered fetal cardiac structure and function [48].

In this study, a single acute exposure to ENM 24-h prior to estrus led to increased inflammatory and vascular dysfunction affecting local nutrient/waste exchange. Alterations to the local uterine environment, including endometrial inflammation and metabolic factors, have been associated with adverse outcomes for patients seeking assisted reproductive treatments and identify them as ‘high risk’ [46]. Infertility literature identifies maternal inflammation as a risk factor for various reproductive disorders [46,47]. These results may also provide evidence of reproductive health effects associated with high PM exposures as ENM are of a similar size range as ultrafine particulate matter (PM 0.1). While PM 0.1 concentrations at a sustained concentration of 10 mg/m^3 are uncommonly high, the outcomes may be of consideration to those who are concerned with infertility, miscarriage, and preconceptive health with long commutes, or who regularly take public transportation in urban areas [3,49,50].

These studies represent the vascular reactivity during a 24-h snapshot during the female reproductive cycle and do not address whether exposure to ENM altered the length of the estrous cycle. Interruptions to the estrous ovulatory cycle were recently reported following pulmonary exposure to multi-walled carbon nanotubes (MWCNT) [51]. These disruptions were found to be stage-dependent, with the greatest effects occurring when exposure took place in the proestrus and estrus stages. Exposures to MWCNT prior to conception have also

been shown to delay litter delivery; however, this outcome has not been consistently observed [51,52]. Implantation in rats can only occur in an amenable uterus, occurring between GD 4 and 6 [53]. Our previous studies indicated microvascular dysfunction would persist for at least 7 days post-exposure [54]. Taken together, these studies may indicate an increased likelihood of impaired fertility and/or reduced implantation rates after ENM exposure. Future studies should thoroughly monitor the estrous cycle timelines and hormonal fluctuations before and after ENM exposure. Additionally, animals in these studies should be allowed to mate during receptive periods to identify any reductions in reproductive rates, maternal weights, litter sizes, pup weights, and gestational timelines occur. Lastly, these exposures represent a single concentrated dose of nano-TiO_2, further dose-dependent studies must be conducted at varying concentrations to address the full impact of ENM pulmonary exposure on female reproductive health.

Overall, these studies revealed: (1) vascular responses using intravital microscopy techniques are not uniform during the stages of estrous and therefore must be taken into account in further analyses, (2) vascular reactivity is disturbed 24-h after a single ENM inhalation exposure during each stage of estrous, and (3) inflammatory status associated with ENM exposure is also influenced by the stage of the female reproductive cycle. Taken together, these outcomes may affect preconceptive health, fertility, and endometrial receptivity.

Acknowledgments

We thank Kevin Engels from the West Virginia University (WVU) Department of Physiology and Pharmacology for his technical assistance in this study, specifically with verification of estrous status, mating of animals, and the fabrication of the intravital microscopy board/platform and Dr. Sara Fournier, Rutgers University EOHSI, for her assistance with data analysis. In addition, we would like to acknowledge our financial support: NIH-R00-ES024783 (PAS), Rutgers Center for Environmental Exposures and Disease (P30-ES005022), Rutgers Joint Graduate Program in Toxicology (T32-ES007148), R01-ES015022 (TRN), and NSF-1003907 (TRN and ABA).

References

1. Pope CA III, Namboodiri MM, Dockery DW, Evans JS, Speizer FE, Heath CW Jr. Particulate air pollution as a predictor of mortality in a prospective study of U. S. adults. Am. J. Respir. Crit. Care Med. 1995; 151(3 (Pt. 1)):669–674. [PubMed: 7881654]
2. Pope CA III, Thurston GD, Thun MJ, Calle EE, Krewski D, Godleski JJ. Cardiovascular mortality and long-term exposure to particulate air pollution: epidemiological evidence of general pathophysiological pathways of disease. Circulation. 2004; 109(1):71–77. [PubMed: 14676145]
3. Frutos V, Gonzalez-Comadran M, Sola I, Jacquemin B, Carreras R, Checa Vizcaino MA. Impact of air pollution on fertility: a systematic review. Gynecol. Endocrinol. 2015; 31(1):7–13. [PubMed: 25212280]
4. Nieuwenhuijsen MJ, Basagana X, Dadvand P, Martinez D, Cirach M, Beelen R, Jacquemin B. Air pollution and human fertility rates. Environ. Int. 2014; 70:9–14. [PubMed: 24879367]
5. Mahalingaiah S, Hart JE, Laden F, Farland LV, Hewlett MM, Chavarro J, Aschengrau A, Missmer SA. Adult air pollution exposure and risk of infertility in the Nurses' Health Study II. Hum. Reprod. 2016; 31(3):638–647. [PubMed: 26724803]
6. Perin PM, Maluf M, Czeresnia CE, Januario DA, Saldiva PH. Impact of short-term preconceptional exposure to particulate air pollution on treatment outcome in couples undergoing in vitro fertilization and embryo transfer (IVF/ET). J. Assist. Reprod. Genet. 2010; 27(7):371–382. [PubMed: 20405197]

7. Perin PM, Maluf M, Czeresnia CE, Nicolosi Foltran Januario DA, Nascimento Saldiva PH. Effects of exposure to high levels of particulate air pollution during the follicular phase of the conception cycle on pregnancy outcome in couples undergoing in vitro fertilization and embryo transfer. Fertil. Steril. 2010; 93(1):301–303. [PubMed: 19631320]
8. Carre J, Gatimel N, Moreau J, Parinaud J, Leandri R. Does air pollution play a role in infertility?: a systematic review. Environ. Health. 2017; 16(1):82. [PubMed: 28754128]
9. Jurewicz J, Radwan M, Sobala W, Polanska K, Radwan P, Jakubowski L, Ulanska A, Hanke W. The relationship between exposure to air pollution and sperm disomy. Environ. Mol. Mutagen. 2015; 56(1):50–59. [PubMed: 24989325]
10. Radwan M, Jurewicz J, Polanska K, Sobala W, Radwan P, Bochenek M, Hanke W. Exposure to ambient air pollution–does it affect semen quality and the level of reproductive hormones? Ann. Hum. Biol. 2016; 43(1):50–56. [PubMed: 26211899]
11. Rengaraj D, Kwon WS, Pang MG. Bioinformatics annotation of human Y chromosome-Encoded protein pathways and interactions. J. Proteome Res. 2015; 14(9):3503–3518. [PubMed: 26279084]
12. Lafuente R, Garcia-Blaquez N, Jacquemin B, Checa MA. Outdoor air pollution and sperm quality. Fertil. Steril. 2016; 106(4):880–896. [PubMed: 27565259]
13. Hougaard KS, Campagnolo L, Chavatte-Palmer P, Tarrade A, Rousseau-Ralliard D, Valentino S, Park MV, de Jong WH, Wolterink G, Piersma AH, Ross BL, Hutchison GR, Hansen JS, Vogel U, Jackson P, Slama R, Pietroiusti A, Cassee FR. A perspective on the developmental toxicity of inhaled nanoparticles. Reprod. Toxicol. 2015; 56:118–140. [PubMed: 26050605]
14. Stapleton PA, Minarchick VC, McCawley M, Knuckles TL, Nurkiewicz TR. Xenobiotic particle exposure and microvascular endpoints: a call to arms. Microcirculation. 2012; 19(2):126–142. [PubMed: 21951337]
15. Nurkiewicz TR, Porter DW, Barger M, Millecchia L, Rao KM, Marvar PJ, Hubbs AF, Castranova V, Boegehold MA. Systemic microvascular dysfunction and inflammation after pulmonary particulate matter exposure. Environ. Health Perspect. 2006; 114(3):412–419. [PubMed: 16507465]
16. Stone V, Johnston H, Clift MJ. Air pollution, ultrafine and nanoparticle toxicology: cellular and molecular interactions. IEEE Trans. Nanobiosci. 2007; 6(4):331–340.
17. Stapleton PA. Gestational nanomaterial exposures: microvascular implications during pregnancy, fetal development and adulthood. J. Physiol. 2016; 594(8):2161–2173. [PubMed: 26332609]
18. Ema M, Hougaard KS, Kishimoto A, Honda K. Reproductive and developmental toxicity of carbon-based nanomaterials: a literature review. Nanotoxicology. 2016; 10(4):391–412. [PubMed: 26375634]
19. Ema M, Kobayashi N, Naya M, Hanai S, Nakanishi J. Reproductive and developmental toxicity studies of manufactured nanomaterials. Reprod. Toxicol. 2010; 30(3):343–352. [PubMed: 20600821]
20. Osol G, Moore LG. Maternal uterine vascular remodeling during pregnancy. Microcirculation. 2014; 21(1):38–47. [PubMed: 23941526]
21. Long, EH., A, J. The Oestrus Cycle in the Rat and Its Associated Phenomena. University of California Press; Berkeley (CA): 1922.
22. Frasier CR, Brown DA, Sloan RC, Hayes B, Stewart LM, Patel HD, Lust RM, Rosenbaum MD. Stage of the estrous cycle does not influence myocardial ischemia-reperfusion injury in rats (Rattus norvegicus). Comp. Med. 2013; 63(5):416–421. [PubMed: 24210018]
23. Stapleton PA, Minarchick VC, Yi J, Engels K, McBride CR, Nurkiewicz TR. Maternal engineered nanomaterial exposure and fetal microvascular function: does the barker hypothesis apply? Am. J. Obstet. Gynecol. 2013; 209(3):227.e1–11. [PubMed: 23643573]
24. Stapleton PA, McBride CR, Yi J, Nurkiewicz TR. Uterine microvascular sensitivity to nanomaterial inhalation: an in vivo assessment. Toxicol. Appl. Pharmacol. 2015; 288(3):420–428. [PubMed: 26375943]
25. Goldman JM, Murr AS, Cooper RL. The rodent estrous cycle: characterization of vaginal cytology and its utility in toxicological studies. Birth Defects Res. B Dev. Reprod. Toxicol. 2007; 80(2):84–97. [PubMed: 17342777]

26. Paccola CC. The rat estrous cycle revisited: a quantitative and qualitative analysis. Anim. Reprod. 2013; 10(4):7.
27. Hathaway QA, Nichols CE, Shepherd DL, Stapleton PA, McLaughlin SL, Stricker JC, Rellick SL, Pinti MV, Abukabda AB, McBride CR, Yi J, Stine SM, Nurkiewicz TR, Hollander JM. Maternal-engineered nanomaterial exposure disrupts progeny cardiac function and bioenergetics. Am. J. Physiol. Heart Circ. Physiol. 2017; 312(3):H446–H458. [PubMed: 28011589]
28. Stapleton PA, Hathaway QA, Nichols CE, Abukabda AB, Pinti MV, Shepherd DL, McBride CR, Yi J, Castranova VC, Hollander JM, Nurkiewicz TR. Maternal engineered nanomaterial inhalation during gestation alters the fetal transcriptome. Part Fibre Toxicol. 2018; 15(1):3. [PubMed: 29321036]
29. Knuckles TL, Yi J, Frazer DG, Leonard HD, Chen BT, Castranova V, Nurkiewicz TR. Nanoparticle inhalation alters systemic arteriolar vasoreactivity through sympathetic and cyclooxygenase-mediated pathways. Nanotoxicology. 2012; 6(7):724–735. [PubMed: 21830860]
30. Nurkiewicz TR, Porter DW, Hubbs AF, Cumpston JL, Chen BT, Frazer DG, Castranova V. Nanoparticle inhalation augments particle-dependent systemic microvascular dysfunction. Part Fibre Toxicol. 2008; 5:1–12. [PubMed: 18269765]
31. Sager TM, Kommineni C, Castranova V. Pulmonary response to intratracheal instillation of ultrafine versus fine titanium dioxide: role of particle surface area. Part Fibre Toxicol. 2008; 5(1): 17. [PubMed: 19046442]
32. Sager TM, Castranova V. Surface area of particle administered versus mass in determining the pulmonary toxicity of ultrafine and fine carbon black: comparison to ultrafine titanium dioxide. Part Fibre Toxicol. 2009; 6:15. [PubMed: 19413904]
33. Yi J, Chen BT, Schwegler-Berry DE, Frazer DG, Castranova V, McBride CR, Knuckles TL, Stapleton PA, Minarchick VC, Nurkiewicz TR. Whole-Body nanoparticle aerosol inhalation exposures. J. Visualized Exp. 2013; (75):e50263.
34. Yi J, Nurkiewicz TR. Nanoparticle Aerosol Generator. 2014
35. Porter DW, Hubbs AF, Chen BT, McKinney W, Mercer RR, Wolfarth MG, Battelli L, Wu N, Sriram K, Leonard S, Andrew M, Willard P, Tsuruoka S, Endo M, Tsukada T, Munekane F, Frazer DG, Castranova V. Acute pulmonary dose-responses to inhaled multi-walled carbon nanotubes. Nanotoxicology. 2013; 7(7):1179–1194. [PubMed: 22881873]
36. Nurkiewicz TR, Porter DW, Barger M, Castranova V, Boegehold MA. Particulate matter exposure impairs systemic microvascular endothelium-dependent dilation. Environ. Health Perspect. 2004; 112(13):1299–1306. [PubMed: 15345343]
37. Nase GP, Boegehold MA. Nitric oxide modulates arteriolar responses to increased sympathetic nerve activity. Am. J. Physiol. 1996; 271:H860–9. [PubMed: 8853318]
38. Leonard S, Lima PD, Croy BA, Murrant CL. Gestational modification of murine spiral arteries does not reduce their drug-induced vasoconstrictive responses in vivo. Biol. Reprod. 2013; 89(6): 139. [PubMed: 24174571]
39. Bohlen HG, Gore RW. Preparation of rat intestinal muscle and mucosa for quantitative microcirculatory studies. Microvasc. Res. 1976; 11(1):103–110. [PubMed: 1263858]
40. Sweeney TE, Bonadio JA, Freiman MA, Getts RT, Lloyd BT, McKeown K, Platt MP, Won JH. A new in vivo microvascular preparation of the hamster ovary. Microcirculation. 1999; 6(4):315–320. [PubMed: 10654282]
41. Schneider CA, Rasband WS, Eliceiri KW. NIH image to ImageJ: 25 years of image analysis. Nat. Methods. 2012; 9(7):671–675. [PubMed: 22930834]
42. LeBlanc AJ, Cumpston JL, Chen BT, Frazer D, Castranova V, Nurkiewicz TR. Nanoparticle inhalation impairs endothelium-dependent vasodilation in subepicardial arterioles. J. Toxicol. Environ. Health A. 2009; 72(24):1576–1584. [PubMed: 20077232]
43. Boegehold MA. Heterogeneity of endothelial function within the circulation. Curr. Opin. Nephrol. Hypertens. 1998; 7(1):71–78. [PubMed: 9442366]
44. Sorokin Y, Romero R, Mele L, Wapner RJ, Iams JD, Dudley DJ, Spong CY, Peaceman AM, Leveno KJ, Harper M, Caritis SN, Miodovnik M, Mercer BM, Thorp JM, O'Sullivan MJ, Ramin SM, Carpenter MW, Rouse DJ, Sibai B. Maternal serum interleukin-6 C-reactive protein, and

matrix metalloproteinase-9 concentrations as risk factors for preterm birth <32 weeks and adverse neonatal outcomes. Am. J. Perinatol. 2010; 27(8):631–640. [PubMed: 20195952]

45. Chatterjee P, Chiasson VL, Bounds KR, Mitchell BM. Regulation of the anti-inflammatory cytokines interleukin-4 and interleukin-10 during pregnancy. Front. Immunol. 2014; 5:253. [PubMed: 24904596]
46. Vannuccini S, Clifton VL, Fraser IS, Taylor HS, Critchley H, Giudice LC, Petraglia F. Infertility and reproductive disorders: impact of hormonal and inflammatory mechanisms on pregnancy outcome. Hum. Reprod. Update. 2016; 22(1):104–115. [PubMed: 26395640]
47. Sheldon IM, Owens SE, Turner ML. Innate immunity and the sensing of infection, damage and danger in the female genital tract. J. Reprod. Immunol. 2017; 119:67–73. [PubMed: 27498991]
48. Velten M, Hutchinson KR, Gorr MW, Wold LE, Lucchesi PA, Rogers LK. Systemic maternal inflammation and neonatal hyperoxia induces remodeling and left ventricular dysfunction in mice. PLoS One. 2011; 6(9):e24544. [PubMed: 21935422]
49. Moreno T, Reche C, Rivas I, Cruz Minguillon M, Martins V, Vargas C, Buonanno G, Parga J, Pandolfi M, Brines M, Ealo M, Sofia Fonseca A, Amato F, Sosa G, Capdevila M, de Miguel E, Querol X, Gibbons W. Urban air quality comparison for bus tram, subway and pedestrian commutes in Barcelona. Environ. Res. 2015; 142:495–510. [PubMed: 26277386]
50. Martins V, Moreno T, Minguillon MC, Amato F, de Miguel E, Capdevila M, Querol X. Exposure to airborne particulate matter in the subway system. Sci. Total Environ. 2015; 511:711–722. [PubMed: 25616190]
51. Johansson HKL, Hansen JS, Elfving B, Lund SP, Kyjovska ZO, Loft S, Barfod KK, Jackson P, Vogel U, Hougaard KS. Airway exposure to multi-walled carbon nanotubes disrupts the female reproductive cycle without affecting pregnancy outcomes in mice. Part. Fibre Toxicol. 2017; 14(1): 17. [PubMed: 28558787]
52. Hougaard KS, Jackson P, Kyjovska ZO, Birkedal RK, De Temmerman PJ, Brunelli A, Verleysen E, Madsen AM, Saber AT, Pojana G, Mast J, Marcomini A, Jensen KA, Wallin H, Szarek J, Mortensen A, Vogel U. Effects of lung exposure to carbon nanotubes on female fertility and pregnancy. A study in mice. Reprod. Toxicol. 2013; 41:86–97. [PubMed: 23714338]
53. Wang H, Dey SK. Roadmap to embryo implantation: clues from mouse models. Nat. Rev. Genet. 2006; 7(3):185–199. [PubMed: 16485018]
54. Stapleton PA, Minarchick VC, Cumpston AM, McKinney W, Chen BT, Sager TM, Frazer DG, Mercer RR, Scabilloni J, Andrew ME, Castranova V, Nurkiewicz TR. Impairment of coronary arteriolar endothelium-dependent dilation after multi-walled carbon nanotube inhalation: a time-course study. Int. J. Mol. Sci. 2012; 13(11):13781–13803. [PubMed: 23203034]

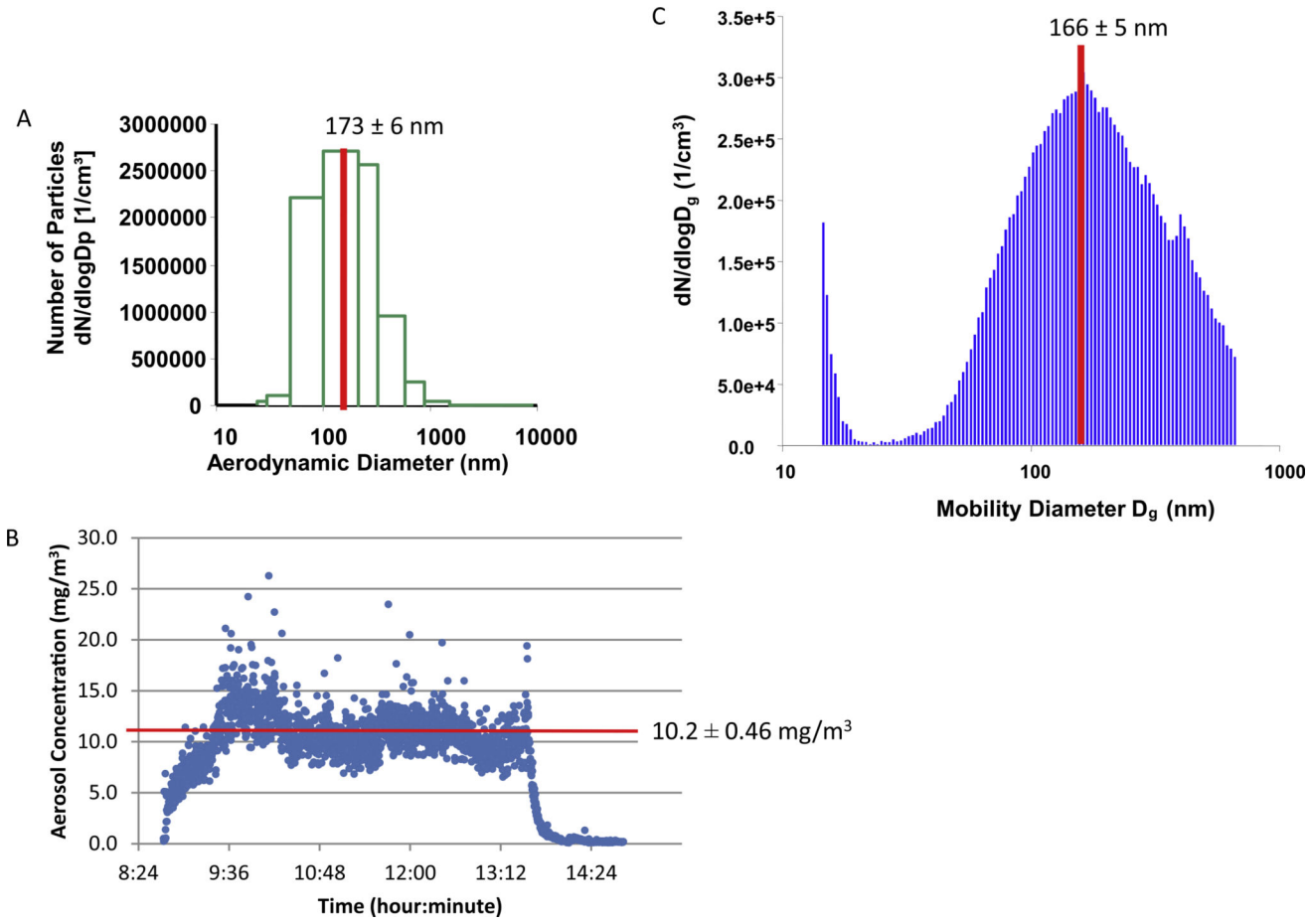

Fig. 1.

Real Time Nano-TiO_2 Exposure Characteristics. (A) Aerosol size distribution and characterization determined by mass-based aerodynamic diameter as a mean of 173 ± 6 nm using ELPI. (B) Size-based aerodynamic diameter and mobility was characterized as 166 ± 5 nm using a SMPS. (C) The daily concentration distribution maintained plateau at 10.2 ± 0.46 mg/m^3. Values are means ± SE.

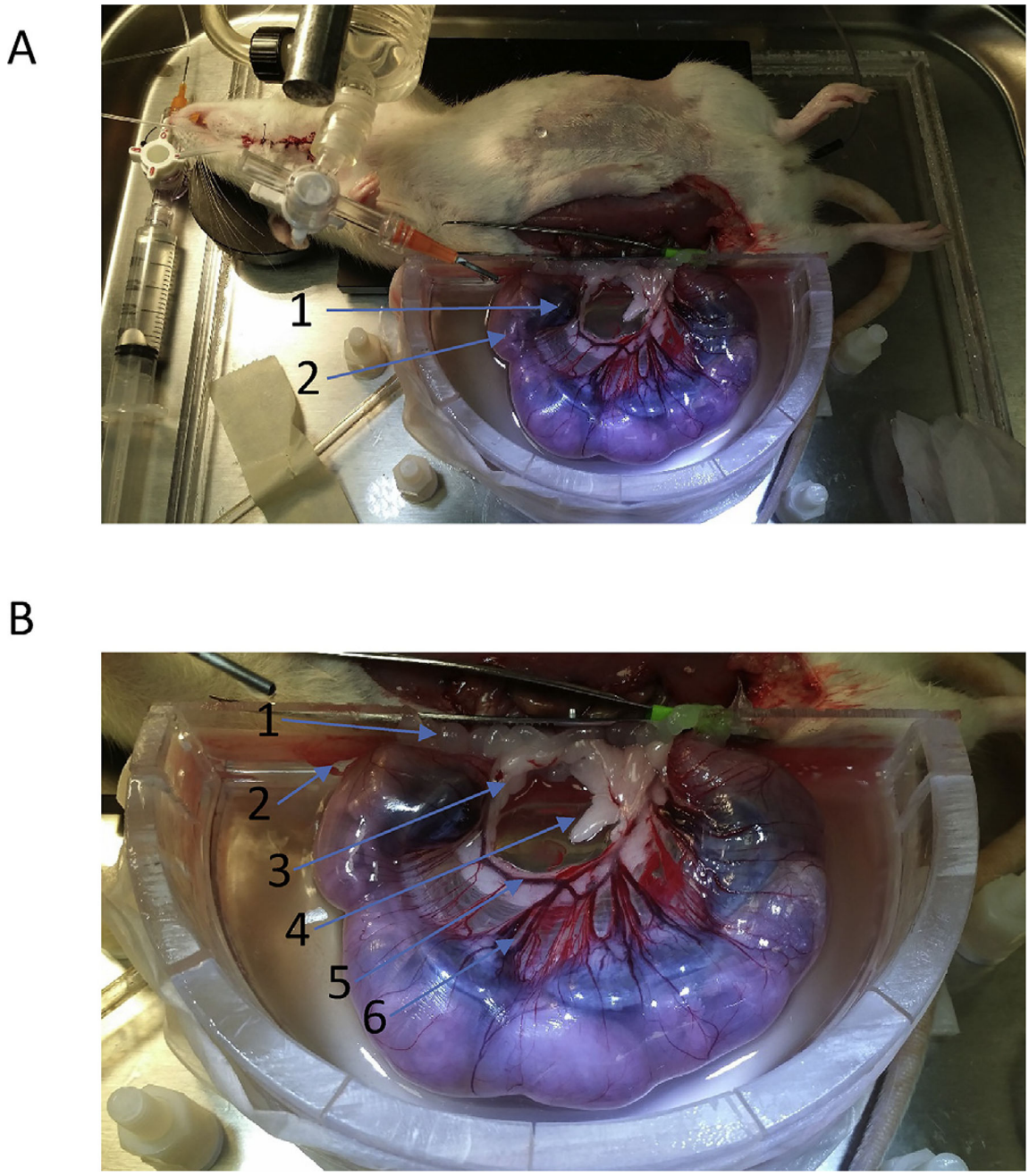

Fig. 2.

Intravital Microscopy Image. (A) Illustration of the late-stage pregnant (GD 20) rat uterus exteriorization. (1) placenta. (2) GD 20 fetal pup. Within this right uterine horn, there are 6 placenta and pup pairs. (B) Identification of uterine antenatal anatomy. (1) placenta, (2) GD 20 fetal pup, (3) uterine artery, (4) arcuate network, (5) radial artery, and (6) basal/straight arterioles.

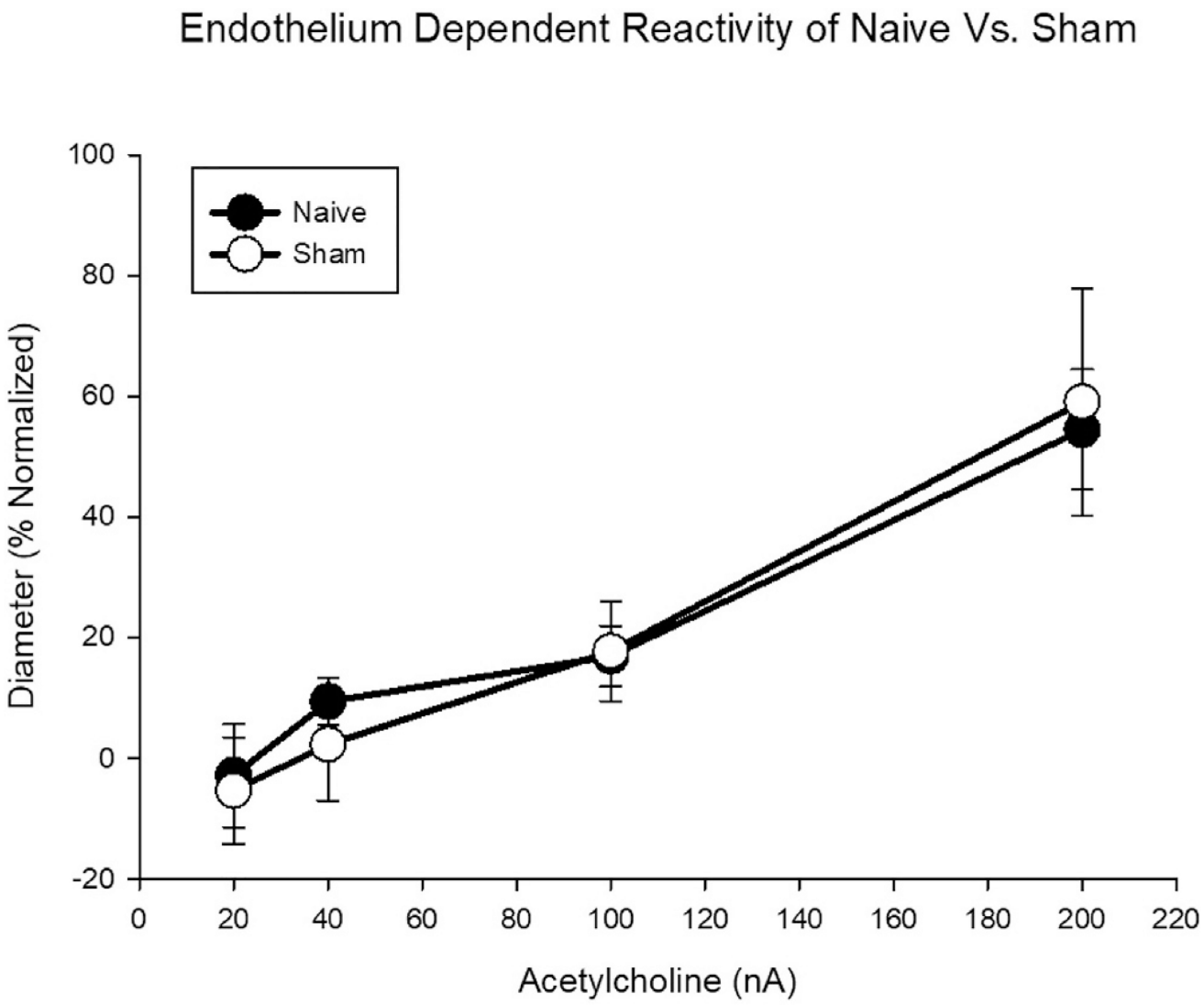

Fig. 3.

Endothelium-dependent arteriolar reactivity of naive and sham (filtered air exposed) control groups. Values are means ± SE.

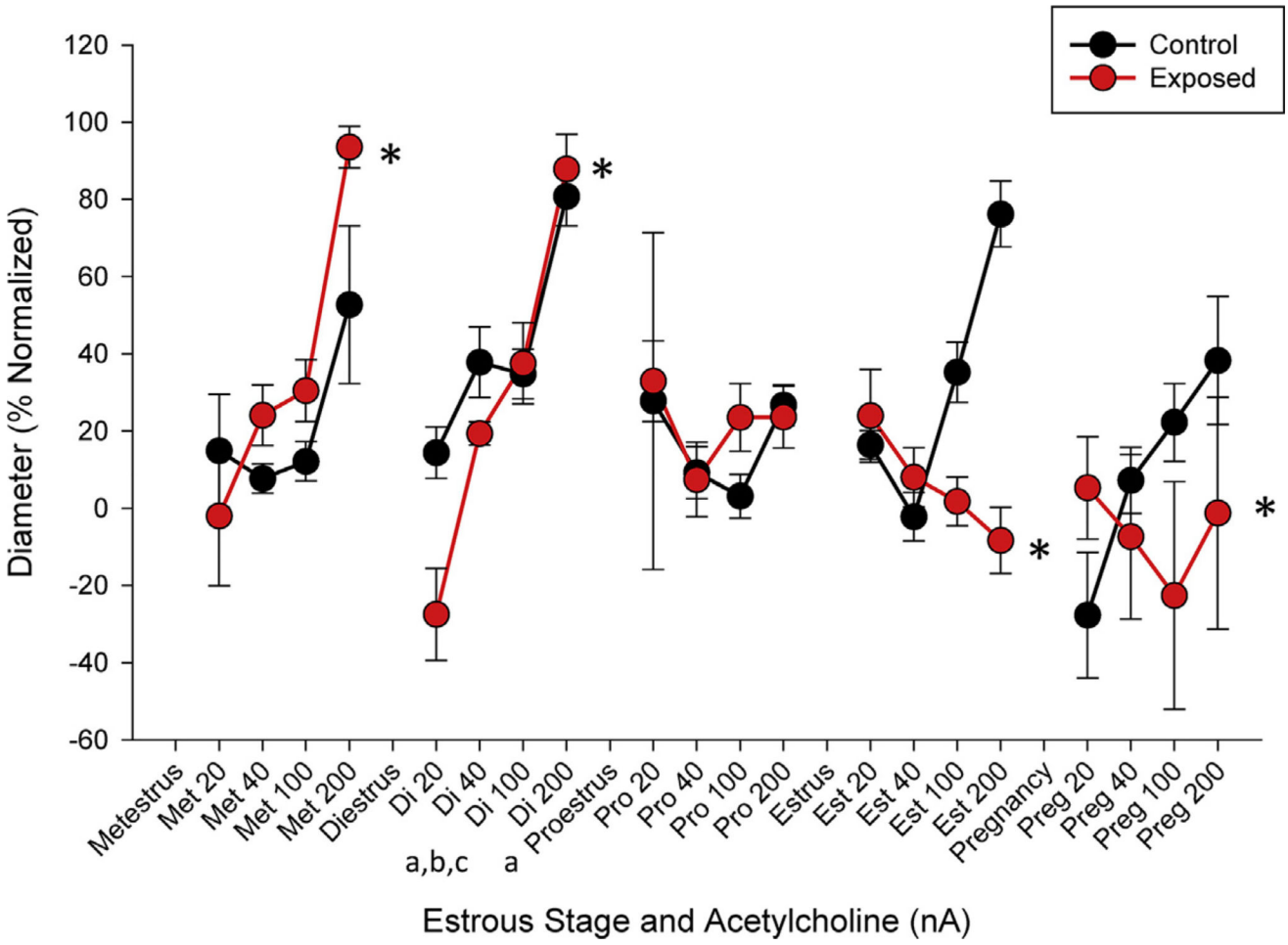

Fig. 4.

Endothelium-dependent arteriolar reactivity normalized to maximum dilation. Measurements are taken in response to increased iontophoretically dosages of acetylcholine between control and exposed groups throughout estrous and late-stage pregnancy. Values are means ±SE. * ($p \leq 0.05$) within group compared to control.[a,b,c] ($p \leq 0.05$) diestrus compared to late-stage pregnancy, estrus, and proestrus stages, respectively.

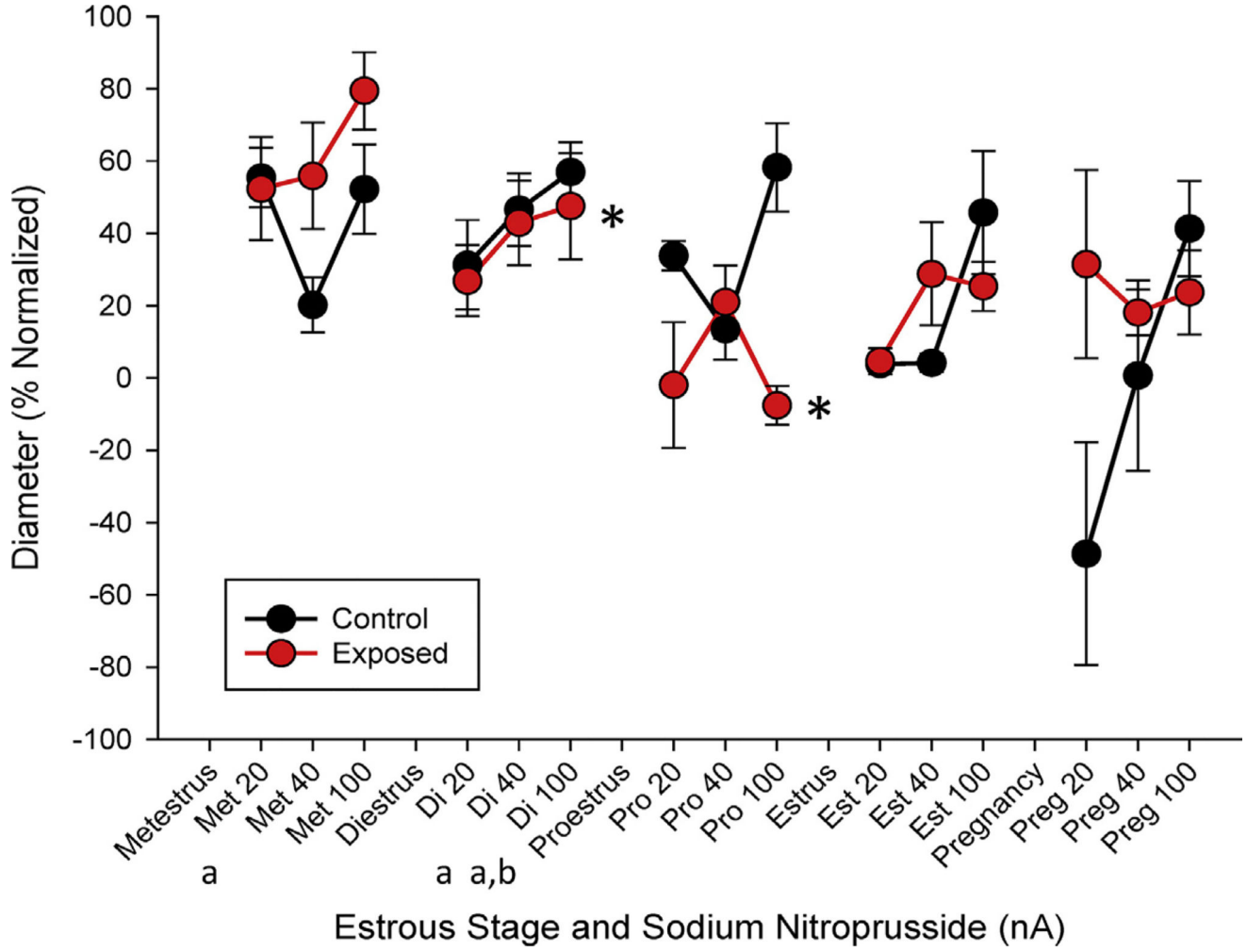

Fig. 5.

Endothelium-independent arteriolar reactivity normalized to maximum dilation. Measurements are taken in response to increased ionic concentrations of sodium nitroprusside. between control and exposed groups throughout estrous and late-stage pregnancy. Values are means ± SE. * ($p \leq 0.05$) within group compared to control.[a,b] ($p \leq 0.05$) compared to late-stage pregnancy and estrus stages, respectively.

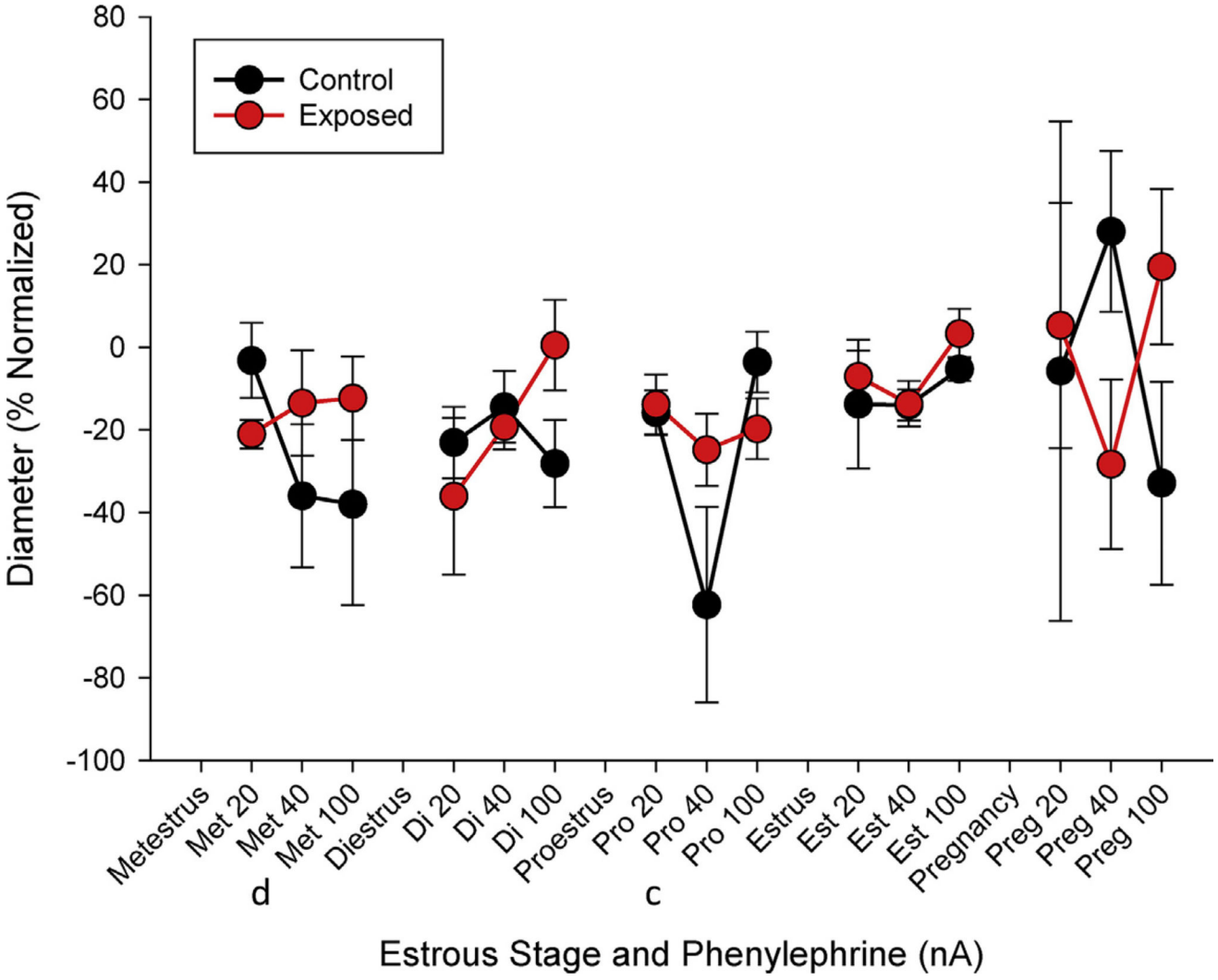

Fig. 6.

Vascular smooth muscle raw (A) and normalized (B) responsiveness between control and exposed groups in response to increased ionic dosages of phenylephrine throughout estrous and late-stage pregnancy. Values are means ± SE. T ($p \leq 0.10$), * ($p \leq 0.05$). ^{c,d} ($p \leq 0.05$) diestrus compared to proestrus and metestrus stages, respectively.

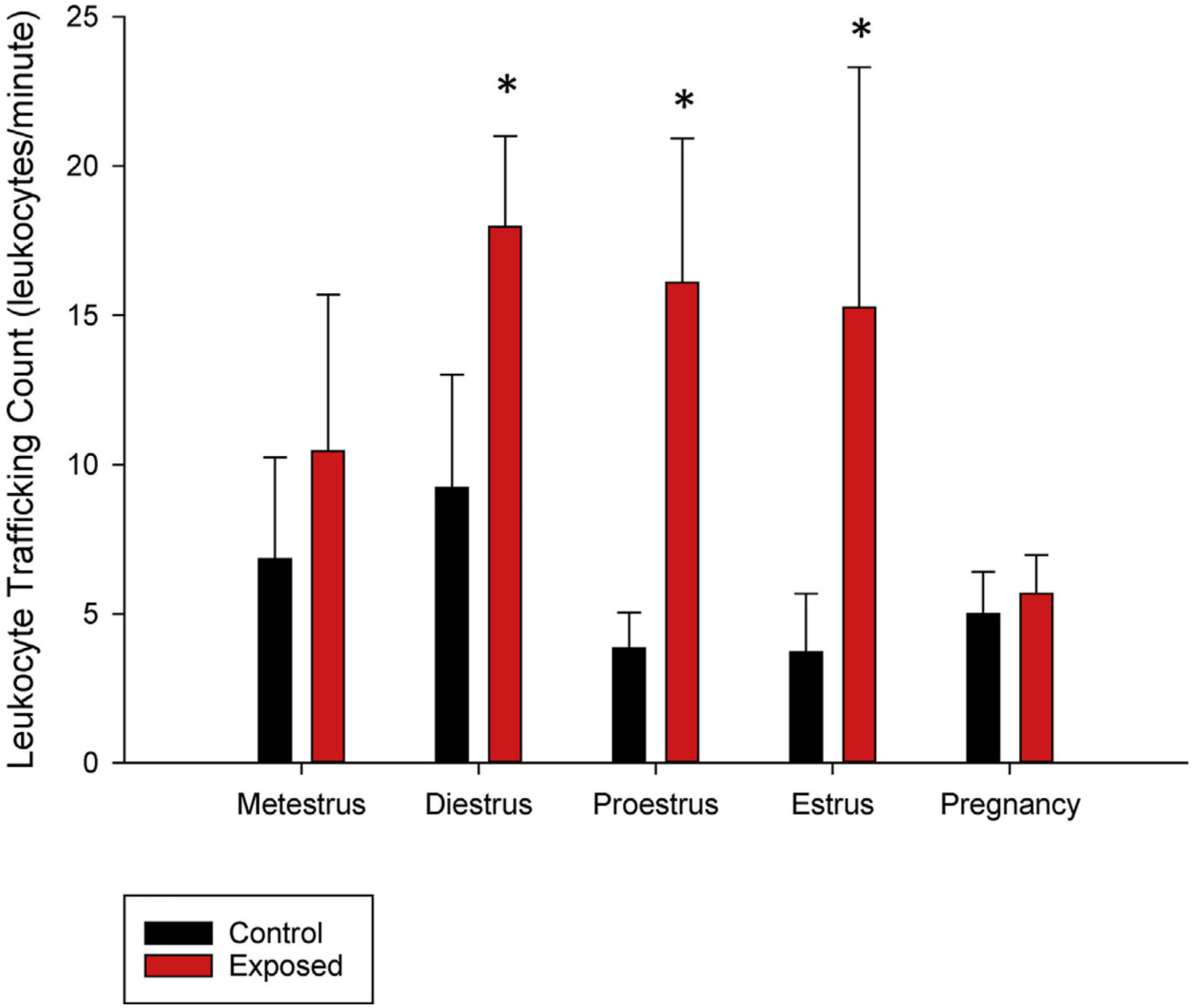

Fig. 7.

Counts of leukocyte adhesion and rolling within small venules at each stage of estrous and late-stage pregnancy 24-h after nano-sized TiO_2 inhalation. Values are means ± SE. * ($p \leq 0.05$).

Table 1

Control and *Exposed* animal and vessel characteristics.

	Metestrus	Diestrus	Proestrus	Estrus	Late-Stage Pregnancy
N (animals)	8	10	5	5	7
	4	*7*	*5*	*7*	*4*
N (vessels)	18	32	9	9	17
	12	*18*	*15*	*13*	*9*
Age	13 ± 1.8	12.25 ± 0.9	14.4 ± 2.7	11 ± 0.4	15.2 ± 1.6
	14 ± 1	*11 ± 1.5*	*13.3 ± 1.9*	*17.3 ± 2.8*	*17.3 ± 0.3*
Weight	246 ± 19	260 ± 9	258 ± 16	252 ± 13	379 ± 23
	280 ± 12	*250 ± 19*	*304 ± 16*	*275 ± 23*	*412 ± 7*
Baseline Diameter (μm)	18.2 ± 2.1	19.9 ± 1.2	14.8 ± 1.4	17.9 ± 1.4	24.3 ± 2.3
	19.6 ± 2.2	*16.5 ± 1.1*	*18.0 ± 1.0*	*19.2 ± 1.8*	*25.1 ± 1.2*
Maximum Diameter (μm)	34.3 ± 2.4	33.7 ± 1.1	29.4 ± 2.0	35.9 ± 1.0	35.2 ± 5.5
	34.3 ± 1.7	*37.8 ± 1.8*	*33.7 ± 1.5*	*38.8 ± 2.2*	*33.1 ± 6.8*

Values are mean ± SE.

* $p \leq 0.05$ vs. Exposed.

Table 2

Results of Two-way ANOVA between exposure groups and within each estrous stage.

Ionic Concentration (μm)	Metestrus	Diestrus	Proestrus	Estrus	Late-Stage Pregnancy
ACh 20 nA	***b***	***b***	***a, b***	***b***	***a, b***
ACh 40 nA	*nd*	***a***	*nd*	*nd*	***a***
ACh 100 nA	*nd*	*nd*	*nd*	*nd*	***a***
ACh 200 nA	*nd*	*nd*	***a***	*nd*	***a***
SNP 20 nA	***c***	*nd*	*nd*	*nd*	***a***
SNP 40 nA	*nd*	*nd*	*nd*	***a***	***a***
SNP 100 nA	***b***	***b***	***b***	***b***	***b***
PE 20 nA	*nd*	*nd*	*nd*	*nd*	*nd*
PE 40 nA	***a, b***	***b***	***a, b***	***b***	***b***
PE 100 nA	*nd*	*nd*	*nd*	*nd*	*nd*

a) $p < 0.05$ vs Diestrus phase,

b) trend toward significance $p < 0.1$ with respect to control vs. exposed group,

c) $p < 0.05$ vs. late-stage pregnancy.

Table 3

Results of two-way ANOVA between exposure and estrous stage for inflammatory markers

Inflammatory Marker (pg/mL)	Metestrus	Diestrus	Proestrus	Estrus	Late-Stage Pregnancy
IL-4	***b***	***b***	***b***	***b***	***b***
IL-6	***T***	***T***	***T***	***T***	***T***
IL-1β	***T***	***T***	***T***	***T***	***T***

b) $p \leq 0.05$ vs. Exposed.

T) indicates a trend toward significance $p < 0.1$.

Table 4

Inflammatory markers (pg.mL).

(pg/ml)	Metestrus	Diestrus	Proestrus	Estrus	Late-Stage Pregnancy
MCP1	10.7 ± 0.7	8.6 ± 1.0	16.2 ± 3.9	6.5 ± 0.3	11.3 ± 3.5
	16.3 ± 3.0	*15.4 ± 4.0*	*5.7 ± 0.6**	*4.9 ± 0.4**	*16.6 ± 4.5*
TIMP-1	48.2 ± 7	50.0 ± 18.7	132.5 ± 34.4	40.5 ± 8.4	29.7 ± 4.0
	36.3 ± 1.3	*21.7 ± 3.7*	*36.8 ± 1.7**	*49.9 ± 7.2*	*44.8 ± 11.9*
Lipocalin-1	275 ± 64	210 ± 55	1009 ± 267	304 ± 107	269 ± 46
	376 ± 125	*85 ± 19**	*271 ± 45**	*1052 ± 585*	*793 ± 339*
TNF-α	33.2 ± 15.8	20.2 ± 6.5	117.5 ± 67.8	9.2 ± 2.7	487.7 ± 312.1
	58.2 ± 20.7	*167.0 ± 61.2**	*73.5 ± 36.2*	*22.6 ± 6.7*	*178 ± 98.6*
KC/GRO	4385 ± 1560	4682 ± 1836	8473 ± 4708	2032 ± 540	2544 ± 537
	1621 ± 272	*5210 ± 1894*	*5324 ± 2698*	*815 ± 157**	*1584 ± 437*
IL-6	7173 ± 2003	8140 ± 1904	43952 ± 20708	19781 ± 770	3424 ± 1221
	6629 ± 2361	*1737 ± 613**	*9131 ± 1288*	*13781 ± 2924**	*251513 ± 78712**
IL-4	1.02 ± 0.28	0.57 ± 0.16	0.53 ± 0.16	0.91 ± 0.32	0.89 ± 0.12
	0.68 ± 0.27	*0.82 ± 0.14*	*1.99 ± 0.52**	*1.39 ± 0.37*	*6.18 ± 2.55**
INF-Ɣ	0.20 ± 0.06	0.13 ± 0.03	0.39 ± 0.17	0.23 ± 0.05	0.32 ± 0.1
	0.19 ± 0.05	*0.31 ± 0.05**	*0.54 ± 0.19*	*0.19 ± 0.03*	*0.05 ± 0.002*

Values are mean ± SE.

* $p < 0.05$.